Electrostatic Debye layer formed at a plasma-liquid interface

Paul Rumbach,[1,*] Jean Pierre Clarke,[1] and David B. Go[1,2,†]

[1]*Department of Aerospace and Mechanical Engineering, University of Notre Dame, Notre Dame, Indiana 46556, USA*

[2]*Department of Chemical and Biomolecular Engineering, University of Notre Dame, Notre Dame, Indiana 46556, USA*

(Received 16 October 2016; revised manuscript received 24 March 2017; published 5 May 2017)

We construct an analytic model for the electrostatic Debye layer formed at a plasma-liquid interface by combining the Gouy-Chapman theory for the liquid with a simple parabolic band model for the plasma sheath. The model predicts a nonlinear scaling between the plasma current density and the solution ionic strength, and we confirmed this behavior with measurements using a liquid-anode plasma. Plots of the measured current density as a function of ionic strength collapse the data and curve fits yield a plasma electron density of $\sim 10^{19}\,\mathrm{m}^{-3}$ and an electric field of $\sim 10^{4}\,\mathrm{V/m}$ on the liquid side of the interface. Because our theory is based firmly on fundamental physics, we believe it can be widely applied to many emerging technologies involving the interaction of low-temperature, nonequilibrium plasma with aqueous media, including plasma medicine and various plasma chemical synthesis techniques.

DOI: 10.1103/PhysRevE.95.053203

I. INTRODUCTION

The electrostatic double layer or Debye layer is a universal phenomenon that occurs at material interfaces. Many mathematical models have been created to describe this phenomenon at various material interfaces including metal-liquid interfaces [1,2], metal-plasma interfaces [3,4], semiconductor junctions [5,6], and ion-selective membranes [7]. These models have been critical to developing much of our modern technology, and devices such as transistors and batteries would not exist without a firm theoretical understanding of the electrostatic Debye layers involved.

To date, there has been very little theoretical work on the Debye layer formed at a plasma-liquid interface, even though interactions between plasmas and aqueous solutions have been experimentally studied for over two centuries. In fact, many important scientific milestones have come as a direct result of these experiments including the repudiation of phlogiston theory [8], the discovery of argon [9], the discovery of ozone [10], and the production of synthetic fertilizers [11]. Plasma-water systems have even been used to simulate the conditions in Earth's primordial oceans, providing insight into the very origin of life itself [12].

Modern methods for producing low-temperature, nonequilibrium plasma at atmospheric pressures in contact with liquids have found many practical applications. For example, the free radicals and UV light they produce can be used to sanitize wastewater [13], treat chronic ulcers [14], and even offer a promising alternative to radiation treatment for various cancers [15]. Several authors have stressed the importance of interfacial electrostatics in these applications. For example, it has been postulated that rate constants in the liquid phase may be altered by a strong electric field [13]. Strong electric fields are also known to induce many biological effects including electroporation [16] and even cause lysing [17]. It has been shown that intense electric fields can kill cancer cells [18], and multiple papers have suggested this as a key mechanism in plasma medicine [19,20].

The electrostatics of any plasma-solution interface should be dictated by the formation of an interfacial Debye layer, where an excess of ions or electrons on the plasma side of the interface is balanced by solvated ions of opposite charge on the liquid side. Despite the rich body of literature on plasma-solution interactions and the universal success of Debye theory for describing most other interfaces, there is currently no working model to describe the electrostatic Debye layer formed at a plasma-solution interface. In this work, we present a simple analytic theory describing the most essential features of the Debye layer formed at the plasma-solution interface of a liquid-anode dc glow discharge and experimentally validate it by measuring the current density as a function of solution ionic strength. Most importantly, our work clearly shows that the electrostatic properties of the interface are highly dependent on the bulk solution chemistry, and specifically the ionic strength.

II. THEORETICAL MODEL

The general framework for our model is a plasma-liquid system where the plasma side is biased negatively relative to the liquid, and the liquid consists of an aqueous solution of an inert salt such as sodium perchlorate ($NaClO_4$) or magnesium sulfate ($MgSO_4$). On the plasma side of the interface, there is a sheath—commonly called an anode fall or anode sheath—that consists almost entirely of electrons diffusing and drifting from the quasineutral bulk plasma region. The coordinate system is defined such that this sheath region begins at $x = 0$ and ends at $x = x_p$ at the solution surface, as shown in Fig. 1. The area to the left of the anode fall is the quasineutral bulk plasma, where ion and electron concentrations are equal, and current is driven by ambipolar diffusion, giving it a slight concentration gradient.

A. Electrostatics

In a liquid-anode configuration, there will be an excess of free electrons and a depletion of positive ions in the anode

*prumbach@nd.edu
†dgo@nd.edu

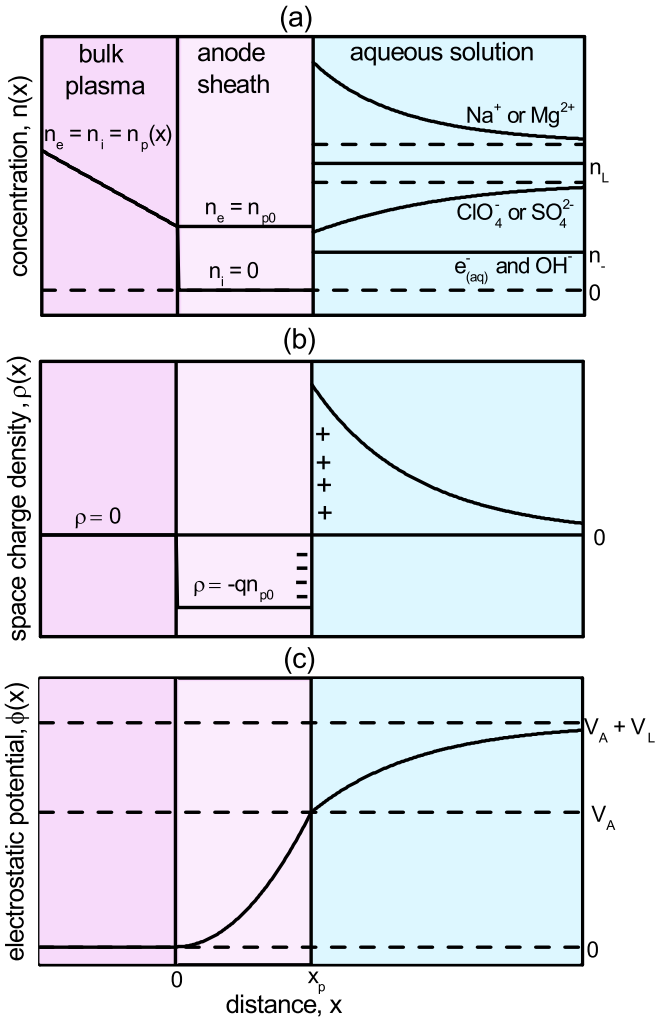

FIG. 1. A sketch of the theoretical distribution of (a) charged species, (b) net space charge, and (c) resultant electrostatic potential profile plotted as a function of distance normal to the interface.

sheath above the liquid surface. The electrostatic potential in this anode sheath is governed by Poisson's equation,

$$\frac{d^2\phi}{dx^2} = \frac{qn_p(x)}{\varepsilon_0}, \tag{1}$$

where q is the charge of an electron, ε_0 is the permittivity of free space, and $n_p(x)$ is the free electron density profile. Expanding $n_p(x)$ as a Taylor series about $x = 0$ yields

$$\frac{d^2\phi}{dx^2} = \frac{q}{\varepsilon_0}\left[n_{p0} + n_p'(0)x + \frac{n_p''(0)x^2}{2} + \cdots\right], \tag{2}$$

where n_{p0} is the free electron density at the sheath boundary at $x = 0$. The first and second derivatives $n_p'(0)$ and $n_p''(0)$ can be determined from the drift-diffusion relation

$$j = qDn_p'(x) + q\mu E(x)n_p(x), \tag{3}$$

where $E(x)$ is the electric field, D is the diffusivity of free electrons, and μ is the mobility of free electrons in the plasma phase. Assuming that the electric field approximately goes to zero in the bulk of the plasma at $x = 0$, and the current density j is spatially uniform and entirely carried by electrons in the anode sheath [21], it follows that $n_p'(0) = j/qD$. Differentiating Eq. (3), solving for $n_p''(x)$ yields, and applying the Einstein relation $D = \mu V_T$ yields the second derivative $n_p''(0) = qn_{p0}^2/V_T\varepsilon_0$, where V_T is the thermal voltage in the plasma. Substituting these formulas for $n_p'(0)$ and $n_p''(0)$ and integrating Eq. (2) yields the electrostatic potential profile

$$\phi(x) = \frac{qn_{p0}x^2}{2\varepsilon_0}\left(1 + \frac{j}{3qDn_{p0}}x + \frac{qn_{p0}}{12V_T\varepsilon_0}x^2 + \cdots\right), \tag{4}$$

where we have imposed the boundary conditions that the potential and electric field go to zero in the bulk plasma at $x = 0$.

In the limit of small current density j and x less than the plasma Debye length $\lambda_p = \sqrt{\frac{\varepsilon_0 V_T}{qn_{p0}}}$, the electrostatic potential profile becomes approximately parabolic,

$$\phi(x) = \frac{qn_{p0}}{2\varepsilon_0}x^2. \tag{5}$$

Thus the total potential dropped across the anode sheath V_A is related to the sheath length x_p by $\phi(x_p) = V_A = \frac{qn_{p0}}{2\varepsilon_0}x_p^2$. This parabolic sheath approximation has been shown to be over 95% accurate under a variety of plasma conditions [22], and it is routinely used in the analysis of semiconductor devices, where it is often referred to as the "parabolic band" assumption [6].

On the solution side of the interface, there are positive cations (i.e., Na^+ or Mg^{2+}) and negative anions (i.e., ClO_4^- or SO_4^{2+}) with a bulk concentration n_L. We will assume the bulk solution is charge neutral with the applied electric field drawing an excess of positively charged cations to the interface, while pushing away the negatively charged anions. The free energy of hydration of the cations is sufficiently large that they remain in the solution in static equilibrium with the electric field. Additionally, there is a column of negative charge extending down from the interface due to the injected plasma electrons, which solvate and recombine to form OH^- [23]. Thus the potential profile is governed by the Poisson-Boltzmann equation,

$$\begin{aligned}\frac{d^2\phi}{dx^2} &= \frac{zqn_L}{\varepsilon_w}\left[\exp\left(\frac{zq\phi}{k_BT_L}\right) - \exp\left(\frac{-zq\phi}{k_BT_L}\right)\right] + \frac{qn_-}{\varepsilon_w} \\ &\approx \frac{\phi}{L_D^2} + \frac{qn_-}{\varepsilon_w},\end{aligned} \tag{6}$$

where z is the integer charge of a given species, $\varepsilon_w = 78\varepsilon_0$ is the permittivity of water, T_L is the liquid temperature, and k_B is the Boltzmann constant, $L_D = \sqrt{\frac{\varepsilon_w k_B T_L}{2q^2 I_S}}$ is the Debye length in the liquid, $I_S = z^2 n_L$ is the ionic strength for a symmetric electrolyte, and $n_- \approx 0.5\,\mathrm{m}M$ is the interfacial concentration of solvated electrons $(e^-)_{aq}$, which recombine to form OH^- anions. Note that we have assumed the negative space charge from $(e^-)_{aq}/OH^-$ is spatially uniform near the interface—an assumption that is approximately in agreement with recent simulations by Gopalakrishnan *et al.* [24].

Solving Eq. (6) and imposing boundedness as $x \to \infty$ yields

$$\phi(x) = -\left(V_L e^{-(x-x_p)/L_D} + \frac{k_BT_l}{2qz^2}\frac{n_-}{n_L}\right), \tag{7}$$

where V_L is the voltage dropped across the liquid side of the interface. In the Gouy-Chapman model, this voltage is a free parameter that must be determined experimentally. For our model, we will assume this parameter is independent of ionic strength, similar to the potential of zero charge (PZC) associated with metallic electrodes [25]. Substituting Eq. (7) into the Boltzmann equation gives us the distribution of positive cations and negative anions in the solution,

$$n_{\pm}(x) = n_L \exp\left(\frac{\pm zq\phi(x)}{k_B T}\right) \approx n_L\left(1 \pm \frac{zqV_L}{k_B T} e^{-(x-x_p)/L_D}\right) \pm \frac{n_-}{2z}. \quad (8)$$

As expected, positive cations such as Na^+ and Mg^{2+} will be drawn up to the liquid surface, while negatively charged anions such as ClO_4^- and SO_4^{2-} will be repelled. Furthermore, the $\pm n_-/2z$ term shows that the negative space charge from the $(e^-)_{aq}/OH^-$ species will be perfectly balanced by both drawing in cations and repelling anions. Effectively, this creates a column of basic NaOH or $Mg(OH)_2$ directly beneath the interface. This phenomenon can be observed using pH sensitive dye, and crystals of $Mg(OH)_2$ can be seen precipitating in solutions of $MgSO_4$, as shown in Fig. 4, which will be discussed further in Sec. III. Recent simulations by Gopalakrishnan *et al.* [24] do not show this phenomenon, likely because their one-dimensional (1D) simulation domain does not allow for radial drift or diffusion of the salt ions to balance the negative charge of $(e^-)_{aq}/OH^-$ species.

To complete the electrostatic model, we apply the matching condition for the displacement field at the plasma-liquid interface, $\varepsilon_0 E_P = \varepsilon_w E_L$. This step is critical to explaining observed plasma phenomena, as it will introduce coupling between the solution chemistry and plasma physics. Applying this boundary condition to Eqs. (5) and (7) yields

$$qn_{p0}x_p = \frac{\varepsilon_w V_L}{L_D}. \quad (9)$$

Further, we see that the plasma anode sheath length x_p and voltage V_A explicitly depend on the bulk salt concentration in the solution n_L. In this way, the chemical properties of the solution have a substantial impact on the electrostatic properties of the discharge. Specifically,

$$x_p = \frac{V_L}{n_{p0}}\sqrt{\frac{2\varepsilon_w z^2 n_L}{k_B T_L}}, \quad (10)$$

and

$$V_A = \frac{\varepsilon_w V_L^2 q z^2 n_L}{\varepsilon_0 n_{p0} k_B T_L}. \quad (11)$$

These three equations essentially show that the electric field at the interface increases with salt concentration n_L, or more specifically the ionic strength $I_S = z^2 n_L$. Importantly, this is consistent with previous studies that have reported that the current density of the solution anode dc glow discharge increases with the ionic strength of the solution [23,26].

B. Current density

The current density of the plasma j will depend on the electrostatics of the interface, which is related to the ionic strength $I_S = z^2 n_L$ as shown in Eqs. (10) and (11). To show this, we utilize analytic techniques commonly used to calculate current-voltage relations in solid-state semiconductor devices to derive an analytic expression for the current density in the plasma j as a function of ionic strength I_S. We first consider the drift-diffusion relation for the electron current density in the anode sheath given by Eq. (3). Again, we will assume the current in the anode sheath is carried entirely by free electrons and not positive ions—an assumption commonly made when modeling glow discharges [21]. Applying the Einstein relation $D = \mu V_T$, Eq. (3) can be written as

$$j = qD\left(\frac{dn_p}{dx} - \frac{1}{V_T}\frac{d\phi}{dx}n_p\right), \quad (12)$$

where $V_T = k_B T_p/q$ is the thermal voltage of the plasma electrons. Multiplying by the integrating factor $\exp(-\phi/V_T)$, we can rewrite Eq. (12) as

$$j \exp\left[\frac{-\phi(x)}{V_T}\right] = qD\frac{d}{dx}\left\{n_p \exp\left[\frac{-\phi(x)}{V_T}\right]\right\}. \quad (13)$$

Substituting Eq. (5), the parabolic potential of the anode fall, and integrating both sides of the equation over the domain $[0, x_p]$ yields

$$j\sqrt{\frac{\pi\varepsilon_0 V_T}{2qn_p}}\,\mathrm{erf}\left(\sqrt{\frac{qn_{p0}}{2\varepsilon_0 V_T}}x_p\right) = qDn_{p0}\left\{1 - \exp\left[\frac{-\phi(x_p)}{V_T}\right]\right\}. \quad (14)$$

Finally, if we substitute Eqs. (10) and (11) into Eq. (14) and rearrange, we arrive at an expression for the current density as a function of ionic strength,

$$j(I_S) = j_\infty \frac{1 - \exp(-\kappa I_S)}{\mathrm{erf}(\sqrt{\kappa I_S})}, \quad (15)$$

where

$$\kappa = \frac{q\varepsilon_w V_L^2}{\varepsilon_0 n_{p0} V_T k_B T_L} \quad (16)$$

is the scale factor for the ionic strength, and

$$j_\infty = D\sqrt{\frac{2q^3 n_{p0}^3}{\pi\varepsilon_0 V_T}} \quad (17)$$

is the maximum current density allowed by the plasma. Equation (15) shows that we anticipate a highly nonlinear scaling of the current density with the ionic strength that also depends on the properties of the plasma itself, namely, the plasma density n_{p0} and electron temperature V_T.

III. EXPERIMENT

To experimentally test the theoretical model, we measured the current density of a liquid-anode dc glow discharge in argon (Ar) gas with solutions of either $NaClO_4$ or $MgSO_4$. The discharge is formed by suspending a sharpened stainless steel capillary (180 μm inner diameter) a distance of 1 or 2 mm above the solution surface. Unlike other similar liquid-anode

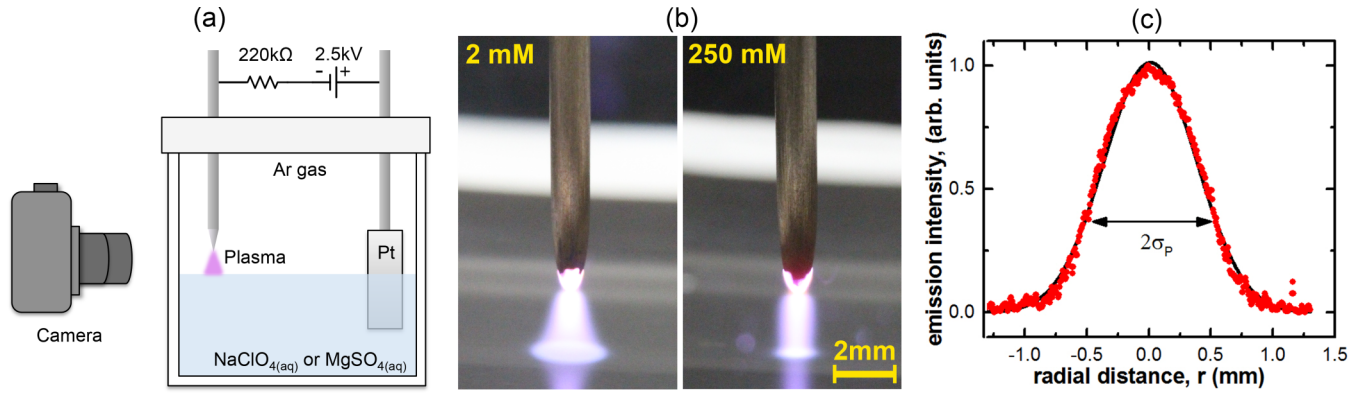

FIG. 2. (a) A schematic of the experimental setup showing the plasma electrochemical cell and camera. Not shown is the microscope and kinematic mounts used for positioning the cathode above the solution surface. (b) Photographs (100 ms exposure) illustrating how the plasma visibly contracts with increasing ionic strength at a fixed plasma current of 10 mA. (c) The optical emission intensity profile at the interface for a 250 mM $NaClO_4$ solution extracted from a digital photograph (25 ms exposure).

discharges, we do not flow gas through the capillary. The gap distance is measured using a digital microscope (Dino-Lite USB Microscope) and set using a micrometer. (Images were calibrated using the known outer diameter of the stainless steel capillary.) The headspace of the reactor is continuously purged with argon (Ar) (99.999% UHP T, Airgas) gas at 200 sccm to eliminate the effects of nitrogen and oxygen chemistry [27]. A grounded piece of platinum foil is submerged in the solution to serve as a counter electrode. The discharge is ignited by applying −2.5 kV dc through a 220-kΩ ballast resistor to the cathode, and the power supply (Glassman, PS/EH05N20L) is operated in a current limited mode at 10 mA. A schematic of the system is shown in Fig. 2(a). Current-voltage (iV) curves measured for the discharge using 200-mM concentrations of both $NaClO_4$ and $MgSO_4$ and gap distances of 1 and 2 mm are shown in Fig. 3. These iV curves exhibit negative differential resistance, which is characteristic of a dc hollow cathode glow discharge in Ar [28].

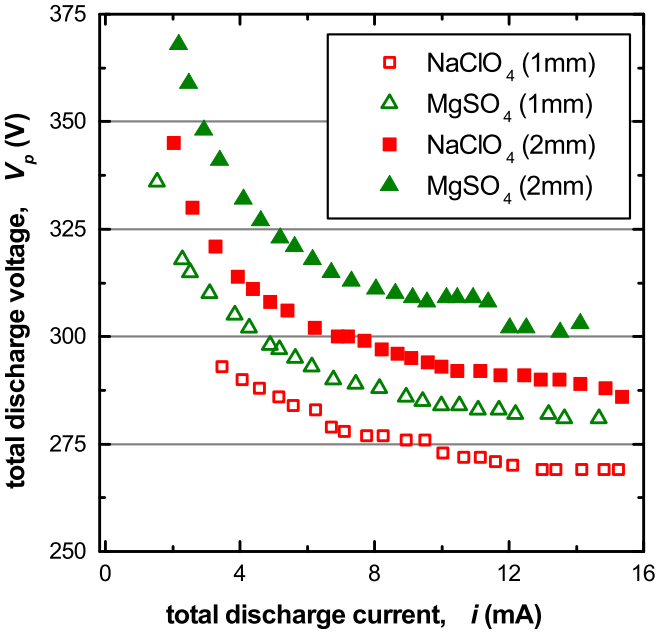

FIG. 3. Current-voltage relations for the discharge for 200 mM solutions of $NaClO_4$ and $MgSO_4$ with gap distances of 1 and 2 mm.

Sodium perchlorate ($NaClO_4$) solutions were prepared by dissolving an appropriate amount of $NaClO_4$ salt ($NaClO_4$, ACS reagent, ⩾98.0%, Sigma Aldrich) into de-ionized water to make batch solutions with concentrations of 20, 200, and 400 mM, which were further diluted to the desired concentrations. Magnesium sulfate ($MgSO_4$) solutions were prepared by diluting concentrated $MgSO_4$ (2.5 M in H_2O, BioUltra, Sigma Aldrich) to make batch solutions with concentrations of 25 and 250 mM, which were further diluted to the desired concentrations. Aliquots of 15 ml of each solution were poured into a 40 × 40 mm cuvette, which was subsequently sealed and purged with Ar for at least 5 min to flush out any air before running the plasma. Figure 4 shows photos of the plasma cell running with solutions of 200 mM $NaClO_4$ and 200 mM $MgSO_4$. A pH sensitive dye (pHydrion one-drop indicator, 1.0 to 11.0) has been added to the $NaClO_4$, which turns dark green under basic conditions. In Fig. 4(a), the dark green column extending down from the plasma-liquid interface is due to the formation of NaOH, as predicted by Eq. (8). For the $MgSO_4$ solution shown in Fig. 4(b), a white precipitate of $Mg(OH)_2$ appears in the solution, as also predicted by the analytical model.

As shown in Fig. 2(b), while holding the current at a constant value $i = 10$ mA, the plasma contracts radially as the salt concentration is increased. Thus the average current density j in the plasma increases with the salt concentration n_L, as qualitatively predicted by the model. We measured this effect by photographing the plasma with a Canon EOS Rebel T3i digital camera and a 100-mm lens using an exposure time of 25 ms and then analyzed the images by extracting the optical emission intensity profile at the interface [Fig. 2(a)]. In Fig. 2(c), one can see that the optical emission intensity profile across the interface appears Gaussian. Assuming the emission intensity is proportional to current density gives us the spatially dependent current density,

$$j(r) = \frac{i}{\pi\sigma_p^2}\exp\left(\frac{-r^2}{\sigma_p^2}\right), \tag{18}$$

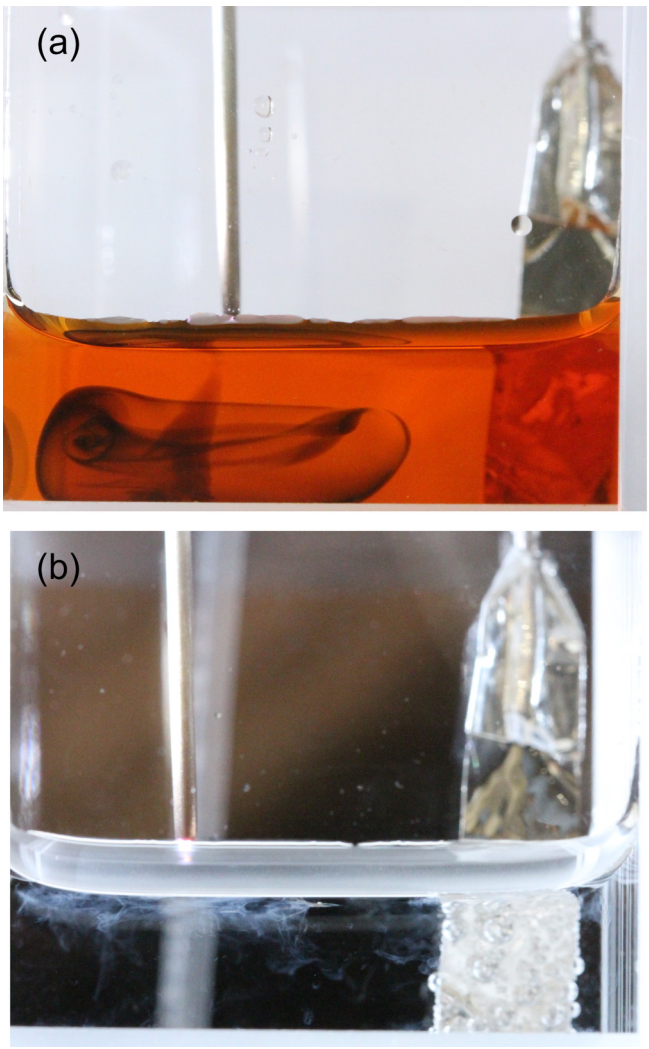

FIG. 4. A photo of the liquid-anode discharge using (a) 200 mM $NaClO_4$ solution containing pH sensitive dye, which turns dark green due to the production of NaOH, and (b) 200 mM $MgSO_4$ solution, which develops a white precipitate due to the production of $Mg(OH)_2$.

where the discharge radius σ_p is determined by applying a Gaussian curve fit to the emission intensity profile with a constant current of $i = 10$ mA. The maximum current density at the center of the discharge is then calculated as

$$j_0 = \frac{i}{\pi \sigma_p^2}. \tag{19}$$

A similar technique was previously used by Lu *et al.* to measure the current density in a liquid electrode ac glow discharge [29]. It should also be noted that others have observed complex pattern formation in similar liquid-anode discharges using high-speed photography [26,30]. These patterns obey the same general trend, where the average radius of the pattern decreases with increasing ionic strength. Importantly, pattern formation typically does not occur at dc currents less than 18 mA, so we expect that our discharge is truly uniform given the low current of 10 mA [26].

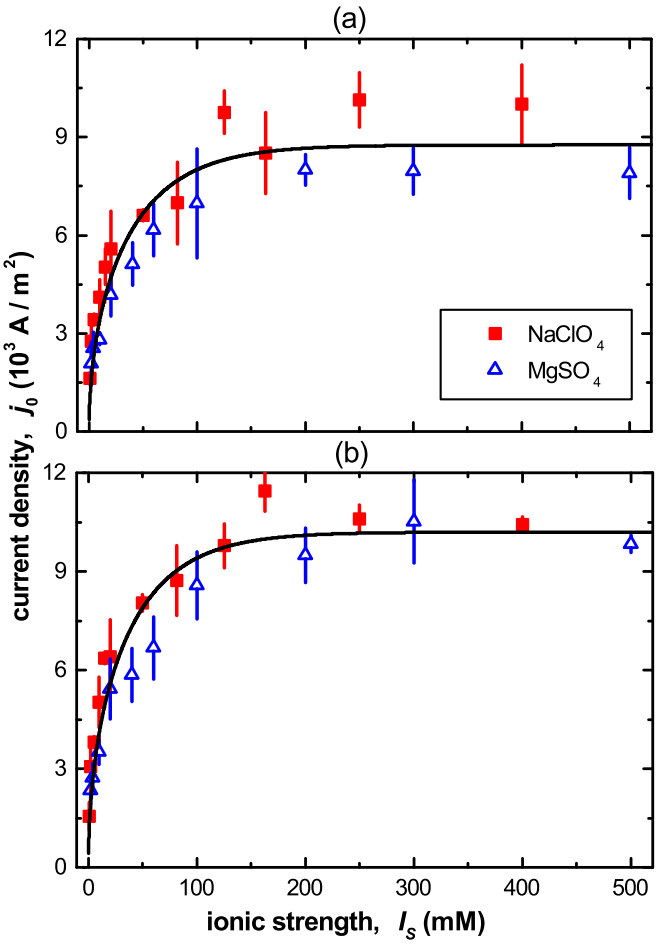

FIG. 5. The measured current density is plotted as a function of ionic strength for monovalent solutions of $NaClO_4$ and divalent solutions of $MgSO_4$ at gap sizes of (a) 1 mm and (b) 2 mm. Solid black lines represent a curve fit using Eq. (15).

IV. RESULTS

Figure 5 shows the measured current density j_0 plotted as function of ionic strength for various concentrations of $MgSO_4$ and $NaClO_4$ with discharge gap distances of 1 and 2 mm. The data points represent the average of at least three different experiments, and the error bars represent the repeatability uncertainty at 70% confidence. As the ions in the two solutions have two different charge states z (e.g., Na^+ vs Mg^{2+}), we can distinguish the impact of ionic strength as opposed to conductivity alone. The measurements agree quite well with Eq. (15), collapsing the data for the two different ionic strengths. We attribute the differences between the two different gap distances to the slight differences in the behavior of the glow discharge as a function of the gap size [31]. In particular, the anode sheath density n_{p0} and thermal voltage of the plasma electrons V_T affect the scale factor κ. We can use the fitting parameters obtained from Fig. 5 to extrapolate the electron density in the anode sheath region n_{p0}. Assuming an electron temperature $V_T = 1.2$ V [32], liquid temperature $T_L = 300$ K, and the diffusivity of plasma electron to be $D = 10^{-3}$ m^2/s in Ar [33], we estimate an electron density of $\sim 10^{19}$ m^{-3}, as shown in Table I. This is consistent with

TABLE I. Parameters obtained from the best-fit curves in Fig. 5 assuming the plasma electron temperature $V_T = 1.2$ V [32], the liquid temperature $T_L = 300$ K, and the diffusivity of plasma electrons $D = 10^{-3}$ m^2/s [33].

	Anode sheath density, n_{p0} (m^{-3})	Liquid voltage V_L (μV)
1 mm	7.5×10^{19}	33
2 mm	6.8×10^{19}	30

experimentally measured values for similar liquid electrode dc glow discharges [34]. Note also that the density decreases with increasing gap distance, as is commonly the case for dc glow discharges [31].

As previously stated, the voltage drop across the liquid side of the interface V_L is a free parameter in the Gouy-Chapman model that must be determined experimentally. Our fitting parameters for Eq. (15) can also be used to determine this value independently from the plasma electron density. Shown in Table I, the voltage drop is around 32 μV for both gap distances. This value may seem small when considering the large voltages associated with the cathode sheath of the plasma. However, it is important to note that the free electrons are hydrophilic, so they will solvate even in the absence of an electrostatic force. Thus little to no electric field is required to drive the free electrons into the liquid-anode solution. For the reversed bias condition—a liquid-cathode discharge—the electric field on the liquid side is likely quite larger, as more energy is required to drive the electrons out of the solution and into the plasma [35].

The extrapolated values of V_L shown in Table I can be used to further estimate the liquid-side electric field at the interface. To calculate the electric field on the liquid side of the interface, we simply take the gradient of Eq. (8), yielding

$$E(x) = -\frac{V_L}{L_D} e^{-(x-x_p)/L_D}. \tag{20}$$

Note that the electric field decays exponentially into the bulk solution with the liquid Debye length L_D as the characteristic distance. Furthermore, the field at the interface E_0 depends on the Debye length, which means it also depends on the ionic strength, such that

$$E_0(I_S) = -V_L \sqrt{\frac{2q^2 I_S}{\varepsilon_w k_B T_L}}. \tag{21}$$

Shown in Fig. 6 is the electric field just beneath the liquid surface, plotted as a function of ionic strength, using the extrapolated values of V_L reported in Table I. Note that the electric field just above the liquid surface, on the anode fall side of the interface, will be a factor of 78 greater due to the dielectric screening of the water. For an ionic strength between 1 and 250 mM, the electric field of $\sim 10^4$ V/m is fairly weak compared to electric fields in traditional electrochemistry, which can be as high as 10^8 V/m [36].

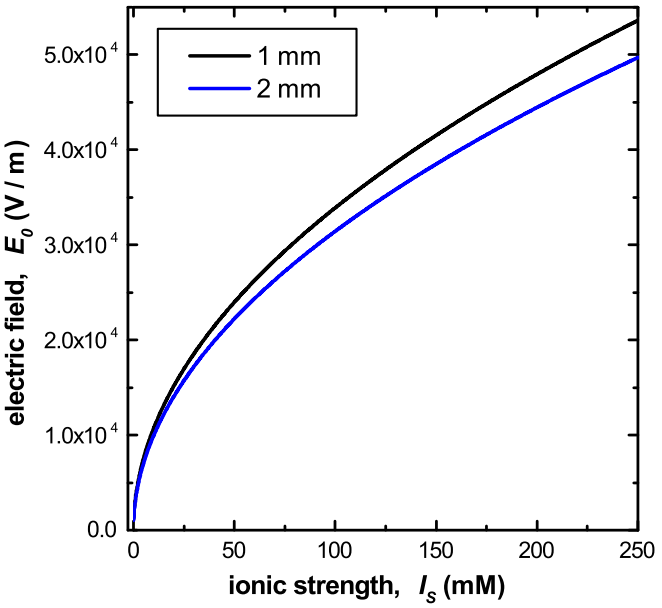

FIG. 6. The electric field just beneath the liquid surface is plotted as a function of ionic strength, using the extrapolated voltage drop of $V_L = 30\,\mu$V and 33 μV across the liquid side of the interface for 1- and 2-mm gaps, respectively.

V. DISCUSSION AND CONCLUSIONS

Our model shows that the electrostatics and charge transport across the interface are highly dependent on the ionic strength of the solution. Under dc conditions, aqueous salt ions significantly screen the electric field, and the liquid Debye length is less than 10 nm for $I_S > 1$ mM. Considering the screening length of the liquid Debye layer, it is apparent that the electric field has little effect on the bulk environment in the quasistatic limit of a dc plasma. Joshi *et al.* suggested that the interfacial electric field may perturb the rate constants of free radicals in the liquid phase [13]. Since most of the free radicals react within 100 nm of the interface, it certainly is possible that the local electric field may perturb the reaction kinetics and transport of these species locally near the interface. However, the electric fields we estimate for our liquid-anode configuration are rather weak, only $\sim 10^4$ V/m, which seems unlikely to perturb any rate coefficients. Additionally, much of the work on electroporation and electric lysing of cells has shown that fields of $\sim 10^6$ V/m [16–18] are required to cause significant damage to cells, which exceeds our estimated field by two orders of magnitude. However, these papers avoided the screening effect of the Debye layer by using short voltage pulses of $\sim$1 ns. The time scale required for the Debye layer to form is $\tau \sim \varepsilon_w/\sigma$, where σ is the solution conductivity [37], and applying high voltages with rise times $\sim$1 ns exposes the cells to the field before the Debye layer has time to form.

In our previous work [23], we had measured the optical absorption spectrum of plasma-injected solvated electrons in a liquid-anode configuration such as that studied here. We observed an apparent blueshift of the spectrum relative to the known spectrum of solvated electrons produced by ionizing radiation. We hypothesized it was either due to a quantum mechanical Stark shift of the electrons' energy states or weakly bound $(e^-)_{aq} - Na^+$ pairs at the interface. However, the extrapolated electric field in this work is about four orders of magnitude too low to yield an appreciable Stark shift. Additionally, Eq. (8) of this work predicts a local concentration

of Na^+ only 1%–2% greater than the bulk, which is not nearly enough to yield the blueshift due to $(e^-)_{aq} - Na^+$ pairs observed by Bonin *et al.* [38] Thus the results presented in this paper negate both of our hypotheses for the blueshift in Ref. [23], leaving the measured difference in the absorption spectrum of plasma solvated electrons an open question.

Lastly, this work has focused on a liquid-anode, dc glow discharge, so it is worth questioning how applicable it is to other plasma-liquid discharge configurations. For example, there are dc liquid-cathode discharges [35,39], ac dielectric barrier discharges [40], pulsed discharges [41,42], and discharges submerged within the liquid [13]. Considering the universal applicability of the Poisson-Boltzmann equation for describing such a wide variety of material interfaces, the same fundamental idea of splicing a plasma sheath to an aqueous Debye layer should still hold. That is, aqueous salt ions should arrange themselves in quasistatic equilibrium with the electric field, and an appropriate matching boundary condition for the field can be applied to initiate coupling between the liquid chemistry and plasma discharge. This quasistatic assumption will, of course, fail when the plasma undergoes temporal changes that are much faster than the diffusive time scales of the aqueous ions, $\tau \sim \varepsilon_w/\sigma$. Such would be the case in sonoluminscent discharges [43] or rf discharges [44]. For ac dielectric barrier discharges, the time scale for the aqueous Debye layer to form would likely induce a phase shift in the current-voltage traces. One could potentially analyze this effect by incorporating the Gouy-Chapman capacitance [25] in an equivalent circuit model.

Overall, it is important to note the universality of the Poisson-Boltzmann equation for modeling the electrostatics of any material interface. We have employed many of the same mathematical techniques and physical principles that were once used for calculating current-voltage relationships in semiconductor devices. Interestingly, Shockley [5] and others based their original semiconductor models on the statistical mechanics of plasmas and the Gouy-Chapman model of liquids. This work has now effectively closed the loop by finally establishing a model for the Debye layer at a plasma-liquid interface. We believe that the essential features of the model should hold for many other types of plasma-liquid interaction, just as the fundamentals contained in Shockley's original work held for a variety of different semiconductor devices. Most importantly, we have shown that the ionic strength of the bulk solution has a substantial impact on the electrostatics of the interface. This is an important result that should be taken into consideration when conducting and analyzing experiments and simulations of plasma-liquid interactions.

ACKNOWLEDGMENTS

P.R. and D.B.G. acknowledge funding from the Electrochemical Society Toyota Young Investigator Fellowship and P.R. acknowledges funding from a ND Energy Postdoctoral Fellowship. We would also like to acknowledge Dr. David Graves and Dr. David Bartels for useful discussions.

[1] M. Gouy, J. Phys. Theor. Appl. **9**, 457 (1910).
[2] D. L. Chapman, London, Edinburgh Dublin Philos. Mag. J. Sci. **25**, 475 (1913).
[3] D. Bohm and E. P. Gross, Phys. Rev. **79**, 992 (1950).
[4] M. A. Lieberman and A. J. Lichtenberg, *Principles of Plasma Discharges and Materials Processing* (Wiley, Hoboken, NJ, 2005).
[5] W. Shockley, Bell Syst. Tech. J. **28**, 435 (1949).
[6] K. Kano, *Semiconductor Devices* (Prentice Hall, Upper Saddle River, NJ, 1998).
[7] H.-C. Chang and L. Y. Yeo, *Electrokinetically Driven Microfluidics and Nanofluidics* (Cambridge University Press, New York, NY, 2010).
[8] H. Cavendish, Philos. Trans. R. Soc. London **74**, 119 (1784).
[9] L. Rayleigh and W. Ramsay, Proc. R. Soc. London **57**, 265 (1895).
[10] C. F. Schönbein, Ann. Phys. (Berlin, Ger.) **126**, 616 (1840).
[11] K. R. Birkeland, Trans. Faraday Soc. **2**, 98 (1906).
[12] S. L. Miller and H. C. Urey, Science **130**, 245 (1959).
[13] A. A. Joshi, B. R. Locke, P. Arce, and W. C. Finney, J. Hazard. Mater. **41**, 3 (1995).
[14] G. Isbary, J. Heinlin, T. Shimizu, J. L. Zimmermann, G. Morfill, H.-U. Schmidt, R. Monetti, B. Steffes, W. Bunk, Y. Li, T. Klaempfl, S. Karrer, M. Landthaler, and W. Stolz, Br. J. Dermatol. **167**, 404 (2012).
[15] M. Keidar, R. Walk, A. Shashurin, P. Srinivasan, A. Sandler, S. Dasgupta, R. Ravi, R. Guerrero-Preston, and B. Trink, Br J. Cancer **105**, 1295 (2011).
[16] R. P. Joshi, Q. Hu, R. Aly, K. H. Schoenbach, and H. P. Hjalmarson, Phys. Rev. E **64**, 011913 (2001).
[17] H. Hulsheger, J. Potel, and E.-G. Niemann, Radiat. Environ. Biophys. **20**, 53 (1981).
[18] R. Nuccitelli, U. Pliquett, X. Chen, W. Ford, R. J. Swanson, S. J. Beebe, J. F. Kolb, and K. H. Schoenbach, Biochem. Biophys. Res. Commun. **343**, 351 (2006).
[19] N. Y. Babaeva, W. Tian, and M. J. Kushner, J. Phys. D: Appl. Phys. **47**, 235201 (2014).
[20] G. Fridman, G. Friedman, A. Gutsol, A. B. Shekhter, V. N. Vasilets, and A. Fridman, Plasma Processes Polym. **5**, 503 (2008).
[21] Y. P. Raizer, *Gas Discharge Physics* (Springer-Verlag, Berlin, 1991).
[22] E. B. Tomme, D. A. Law, B. M. Annaratone, and J. E. Allen, Phys. Rev. Lett. **85**, 2518 (2000).
[23] P. Rumbach, D. M. Bartels, R. M. Sankaran, and D. B. Go, Nat. Commun. **6**, 7248 (2015).
[24] R. Gopalakrishnan, E. Kawamura, A. J. Lichtenberg, M. A. Lieberman, and D. B. Graves, J. Phys. D: Appl. Phys. **49**, 295205 (2016).
[25] W. Schmickler and E. Santos, *Interfacial Electrochemistry* (Springer, Verlag, 2010).
[26] T. Verreycken, P. Bruggeman, and C. Leys, J. Appl. Phys. **105**, 083312 (2009).
[27] P. Rumbach, D. M. Bartels, R. M. Sankaran, and D. B. Go, J. Phys. D: Appl. Phys. **48**, 424001 (2015).

[28] R. H. Stark and K. H. Schoenbach, J. Appl. Phys. **85**, 2075 (1999).
[29] X. P. Lu, F. Leipold, and M. Laroussi, J. Phys. D: Appl. Phys. **36**, 2662 (2003).
[30] N. Shirai, S. Uchida, and F. Tochikubo, Plasma Sources Sci. Technol. **23**, 054010 (2014).
[31] A. L. Ward, Phys. Rev. **112**, 1852 (1958).
[32] V. A. Titov, V. V. Rybkin, S. A. Smirnov, A. L. Kulentsan, and H.-S. Choi, Plasma Chem. Plasma Process. **26**, 543 (2006).
[33] M. McFarland, D. L. Albritton, F. C. Fehsenfeld, E. E. Ferguson, and A. L. Schmeltekopf, J. Chem. Phys. **59**, 6610 (1973).
[34] P. Bruggeman and C. Leys, J. Phys. D: Appl. Phys. **42**, 053001 (2009).
[35] P. Mezei and T. Cserfalvi, Appl. Spectrosc. Rev. **42**, 573 (2007).
[36] P. Delahay, *Double Layer and Electrode Kinetics* (Interscience Publishers, Geneva, Switzerland, 1965).
[37] P. Šunka, Phys. Plasma **8**, 2587 (2001).
[38] J. Bonin, I. Lampre, and M. Mostafavi, Radiat. Phys. Chem. **74**, 288 (2005).
[39] A. J. Schwartz, S. J. Ray, G. C.-Y. Chan, and G. M. Hieftje, Spectrochim. Acta, Part B **125**, 168 (2016).
[40] G. Fridman, M. Peddinghaus, H. Ayan, A. Fridman, M. Balasubramanian, A. Gutsol, A. Brooks, and G. Friedman, Plasma Chem. Plasma Process. **26**, 425 (2006).
[41] C. E. Anderson, N. R. Cha, A. D. Lindsay, D. S. Clark, and D. B. Graves, Plasma Chem. Plasma Process. **36**, 1393 (2016).
[42] A. M. Lietz and M. J. Kushner, J. Phys. D: Appl. Phys. **49**, 425204 (2016).
[43] B. Gompf, R. Günther, G. Nick, R. Pecha, and W. Eisenmenger, Phys. Rev. Lett. **79**, 1405 (1997).
[44] Q. Chen, K. Saito, Y.-I. Takemura, and H. Shirai, Thin Solid Films **516**, 6688 (2007).